245Gb/s P2MP Mobile Fronthaul Downstream Transmission Using Code-Division Multiplexing and Self-Homodyne Coherent Technologies

Xiaoyang Liu, Longquan Dai, Chuanming Huang, Mengfan Cheng, *Senior Member, IEEE*, Qi Yang, *Senior Member, IEEE*, Ming Tang, *Senior Member, IEEE*, Deming Liu, and Lei Deng, *Senior Member, IEEE*

***Abstract*—We have proposed and experimentally demonstrated a high-speed and point-to-multipoint (P2MP) mobile fronthaul (MFH) downstream system based on the code-division multiplexing (CDM) and self-homodyne coherent (SHC) technologies. We find that compared with the traditional 16-ary quadrature amplitude modulation (16-QAM) signal transmission, the change of phase noise between two demultiplexed symbols is much larger in the CDM-16QAM signal transmission because it is the accumulation of phase noise change of n multiplexed symbols. Therefore, a low-complexity pilot sequence-assisted phase noise estimation algorithm is proposed and designed to compensate for the phase noise caused by fiber mismatch length, which makes it possible to use a low-cost distributed feedback (DFB) laser. Besides, the spread signal's distribution in the frequency domain of each code sequence is different, leading to different transmission performances between different remote radio units (RRUs). A power optimization scheme is proposed to balance the transmission performances of different RRUs by multiplying each channel's signal by a normalized weight factor at the transmitter. The experimental results show that the proposed system could successfully support the transmission of 245 Gb/s 16QAM signal from baseband unit (BBU) to 7 RRUs (each RRU could have 2 antennas to transmit signals at 2 polarizations) over 10 km standard single-mode fiber (SSMF). The measured worst bit error rate (BER) value of 14 channels is 1.77e-3 which is below the hard-decision forward error correction (HD-FEC) threshold (3.8e-3).**

***Index Terms*—Mobile fronthaul (MFH), code-division multiplexing (CDM), self-homodyne coherent (SHC).**

I. Introduction

TO MEET the requirements of the 5th generation mobile communication (5G) for high data rate, low latency, and a large number of devices as well as reduced capital expenditures for operators, the centralized radio access network (C-RAN) has emerged [1], [2]. In C-RAN, the communication link between the baseband unit (BBU) and remote radio units (RRUs) is denoted as mobile fronthaul (MFH) [3]. Normally, the MFH transmission could be categorized into analog radio over fiber (A-RoF) and digital radio over fiber (D-RoF) transmission. A-RoF can achieve high spectral efficiency because it directly transmits analog signals and doesn't need an up-conversion operation at the RRU. However, A-RoF will impose high linearity requirements on optical and electrical components, and it is more sensitive to optoelectronic noise and impairment in the transmission link [4]. As for D-RoF, though it has lower spectral efficiency compared with the A-RoF, it can achieve high signal fidelity because transmitting digital quantized signal can mitigate the non-linearity issues in both BBU and RRU. So, it is still a promising scheme for the MFH, and many D-RoF standards already exist such as common public radio interface (CPRI). In the MFH system, the BBU needs to communicate with more than one RRU simultaneously [5]. Therefore, the MFH downstream will be split into separate transceiver systems, which causes increased cost and system complexity. To cope with this problem, point-to-multipoint (P2MP) technology is introduced, such as time-division multiplexing (TDM), wavelength-division multiplexing (WDM), space-division multiplexing (SDM), frequency-division multiplexing (FDM), and code-division multiplexing (CDM) technologies. By using the multiplexing technology, only one transmitter is needed in BBU, and the separate channels could be combined and transmitted in a single fiber. On the remote side, the multiplexed signal will be transmitted to every RRU by an optical splitter. WDM technology is widely used in P2MP systems, which can support the transmission with high speed, low latency, and multiple users. However, WDM requires strict wavelength control which could reduce the tunability of the MFH system [6], [7]. Besides, as each RRU needs one specific wavelength for communication [8], additional hardware support is inevitable. Therefore, the use of WDM will lead to high system costs. For SDM, it is realized by establishing multiple spatially distinguishable channels in a single fiber [9]. Similar to WDM, it also has the advantages of large capacity and low latency, but SDM relies on multi-core and few-mode fiber, which is not compatible with the current

Manuscript received 9 October 2022; accepted 15 October 2022. Date of publication 19 October 2022; date of current version 2 November 2022. This work was supported in part by the National Key Research and Development Program of China under Grant 2018YFB1800903 and in part by the National Nature Science Foundation of China (NSFC) under Grant 62171190. *(Corresponding author: Lei Deng.)*

The authors are with the Wuhan National Laboratory for Optoelectronics and School of Optical and Electronic Information, Huazhong University of Science and Technology, Wuhan 430074, China (e-mail: m202172906@hust.edu.cn; d202080779@hust.edu.cn; hust_hcm@hust.edu.cn; chengmf@mail.hust.edu.cn; yangqi@hust.edu.cn; tangming@mail.hust.edu.cn; dmliu@mail.hust.edu.cn; denglei_hust@mail.hust.edu.cn).

Digital Object Identifier 10.1109/JPHOT.2022.3215473

fiber network. And the fan-in and fan-out devices are still not commercially available [10], which limits the application of SDM in MFH. Compared with the mentioned WDM and SDM, the TDM system has a simpler structure, lower cost, and can support a large number of devices at the same time. However, the latency of TDM may limit its application in 5G MFH. Though several kinds of research focused on reducing latency are carried out recently [11], [12], the latency will increase with the number of RRUs. The FDM technology seems like a promising solution due to its advantage of low complexity and efficient realization of multiple users [13]. The multiplexing of FDM could be carried out in the optical domain or digital domain. The optical-domain demultiplexing relies on the alignment of the local oscillator (LO) frequency and the subcarrier's center frequency. Therefore, a frequency-tunable laser is required to ensure the flexibility of the system and the frequency offset must be controlled accurately to avoid the crosstalk between adjacent subchannels, which means a complexity increase of the RRUs. The digital-domain complexing could be realized in DSP by capturing the full band. It does not need additional hardware devices and could be combined with the self-homodyne coherent technology to reduce the cost. Therefore, the following comparisons between CDM and FDM are based on digital-domain complexing. The demultiplexing process of FDM relays on the digital filter or fast Fourier transformation/inverse fast Fourier transformation (FFT/IFFT), which will consume a large part of computing resources in the DSP [14]. Besides, the insertion of guard bands will cause a reduction in spectral efficiency [15]. At the same time, the transmission performance of different FDM channels will vary greatly because the amplitude-frequency response is not flat in the bandwidth. Therefore, different channels of FDM usually transmit signals with different modulation formats to achieve the bit error rate (BER) requirement [16]. CDM technology is widely used in mobile communication because of its advantages of multiple users, low latency, and low complexity. The multiplexing and demultiplexing process of CDM can be easily realized in the digital domain just by addition or subtraction operations [17], [18] and does not need additional hardware devices. Meanwhile, CDM has no special requirements for transceivers and transmission links. Therefore, it can be compatible with the current fiber network. Moreover, CDM has lower latency in theory compared with TDM. Therefore, in some cost-sensitive scenarios in the MFH, the CDM-based P2MP downstream scheme could be a promising solution with its advantages of low complexity and high spectral efficiency.

The low spectral efficiency of D-RoF is mainly caused by the digital quantization procedure and the mainstream binary ON-OFF-keying modulation format [19]. So, the introduction of high-order modulation formats such as coherent detection-enabled 16-QAM can effectively increase spectral efficiency. However, the introduction of coherent detection will cause a non-negligible increase in the cost and complexity of the RRU. To cope with this problem, self-homodyne coherent (SHC) technology is introduced. In recent years, SHC optical transmission technology is widely studied for the short- to medium-reach optical communication systems. In the SHC system, the LO is transmitted originally from the transmitter laser to the receiver [20], [21]. The SHC technology can relax the requirement for narrow-linewidth lasers and simplify the carrier phase recovery (CPR), contributing to reducing the system cost greatly [22]. Therefore, it is a promising solution for the MFH. However, the phase noise induced by laser linewidth and fiber length mismatch between the signal and LO paths still impacts the SHC system. The phase noise increases with the increasing production of laser linewidth and mismatch length [23], [24]. Due to the independent transmission in two fibers, the mismatch length between the signal and LO paths cannot be eliminated completely in practice, especially when a low-cost and large-linewidth distributed feedback (DFB) laser is used. In this case, a simple CPR algorithm is still required for the SHC system. The influence of phase noise behaves as the phase change (delta phase noise) between adjacent symbols, and the time interval between two adjacent detected symbols is usually the reciprocal of the baud rate. However, when the CDM technology is used in the SHC system, the time interval between two adjacent signal symbols is N times the transmitting symbols due to the multiplexing operation, where N depends on the number of multiplexed channels. In other words, the phase change between adjacent symbols after demultiplexing is N times that before demultiplexing, and the effect of phase noise is also N times that in the traditional SHC system. Moreover, the CPR in the CDM-based SHC-MFH system must be carried out after the demultiplexing, because the detected CDM signal is not a standard QAM signal, which means the widely used blind phase search (BPS) algorithm [25] doesn't work. Therefore, a novel CPR algorithm is highly desired for the CDM-based SHC-MFH system.

In this paper, we demonstrate a low-cost, high-speed, and P2MP DRoF-MFH downstream transmission by using the CDM and SHC technologies. A low-complexity phase noise estimation algorithm is proposed to increase the fiber length mismatch tolerance when a low-cost and large-linewidth DFB laser is used. Besides, the orthogonal Gold code is introduced and a power optimization scheme is designed for ensuring the balance of transmission performances between different RRUs. By this means, a 245 Gb/s CDM-based MFH downstream transmission from BBU to 7 RRUs (each RRU has 2 antennas to transmit signals at 2 polarizations) over 10 km standard single-mode fiber (SSMF) is carried out. The linewidth of the used DFB laser is 4 MHz, and the bit rate of each RRU is 35 Gb/s (17.5 Gb/s for each antenna). The measured worst BER performance of 14 channels is 1.77e-3 which is below the hard-decision forward error correction (HD-FEC) threshold (3.8e-3).

II. Principle

A. Comparison Between the CDM and FDM Technologies

As mentioned above, both the CDM and FDM are promising schemes for the P2MP DRoF-MFH system. In the FDM scheme, each RRU has a subcarrier for transmission as shown in Fig. 1(b). Usually, to avoid the crosstalk between adjacent subcarriers, the insertion of guard bands is necessary. And the transmission performance will increase with the broadening of guard bands. However, the broadening of guard bands also means the reduction of spectral efficiency. The trade-off between the

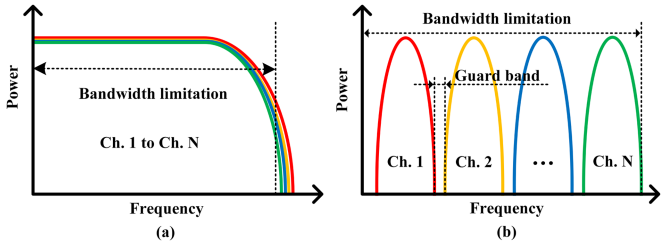

Fig. 1. Comparison of spectral efficiency between the CDM technology (a) and the FDM technology (b).

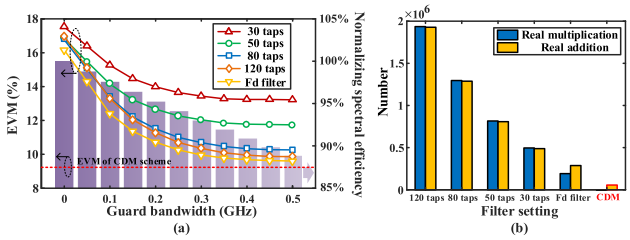

Fig. 2. The measured average EVM performance of 8 RRUs with different filters and normalizing spectral efficiency in terms of different guard bandwidths (a). The demultiplexing required number of real multiplications and real additions with different filter settings or with CDM (b).

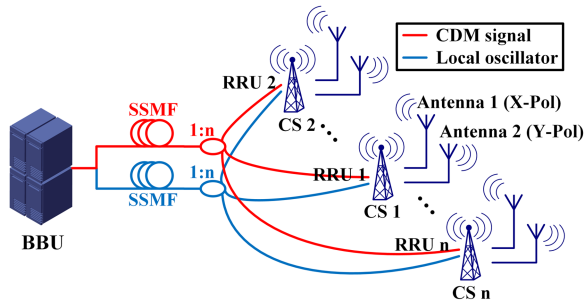

Fig. 3. The structure of the proposed P2MP MFH downstream transmission used the CDM and SHC technologies.

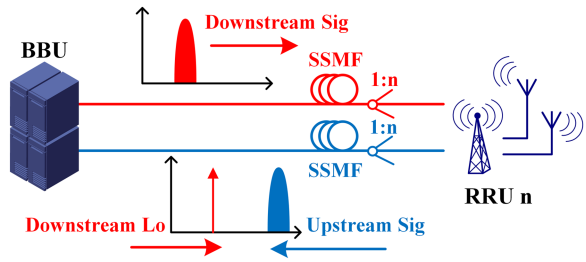

Fig. 4. The structure of the bidirectional transmission system used the SHC technology.

transmission performance and the spectral efficiency must be considered.

To demonstrate the demultiplexing complexity and spectral efficiency differences between FDM and CDM schemes, a 32 GBaud 16QAM signal SHC optical back-to-back (OBTB) transmission simulation using Matlab and VPI Transmission.

Maker 9.9 is carried out. 4000 16QAM symbols are transmitted. The optical signal noise ratio (OSNR) is set to 25 dB. In this simulation, the BBU will communicate with 8 RRUs, the bit rate of each RRU is 16 Gbps (4 GBaud $\times$ 4 bit/symbol). For CDM, the used code is an 8-bit orthogonal Gold code. For FDM, 8 subcarriers are generated and each one is modulated at 4GBaud with Nyquist pulse shaping (the roll-off factor is 0.1). The initial interval of subcarriers is 4 GHz and the guard bandwidth is set from 0 Hz to 0.5 GHz. The FFT-based filter and time-domain filter (Hamming Window based) with different taps (30, 50, 80, and 120) are compared.

Fig. 2(a) shows the average error vector magnitude (EVM) performance of 8 RRUs using different filters and the normalizing spectral efficiency (the spectral efficiency of CDM is denoted as 100%) in terms of different guard bandwidths. The measured EVM value becomes small with the broadening of the guard band because larger guard bandwidth can avoid the crosstalk between subcarriers more effectively. However, larger guard bandwidth also means lower spectral efficiency. In this transmission, nearly the best EVM performance could be obtained when the guard bandwidth reaches 0.35 GHz, and the spectral efficiency is only 92% of CDM at this moment. Meanwhile, the EVM value also becomes small with the increase of time-domain filter taps and the best EVM performance could be obtained by using the FFT-based filter. The demultiplexing required number of real multiplications and real additions using different filters or with CDM is shown in Fig. 2(b). The complexity of the time-domain filter is much higher than the FFT-based filter. However, the demultiplexing complexity of CDM is much lower, only a small number of real additions are required. Therefore, in some cost-sensitive MFH scenarios, the CDM scheme is more suitable for the MFH system due to its higher spectral efficiency and lower complexity of demultiplexing compared with the FDM scheme.

B. The P2MP MFH Downstream Transmission Based on CDM and SHC Technologies

The structure of the proposed P2MP MFH downstream transmission is shown in Fig. 3. The BBU can communicate with n RRUs simultaneously with the help of polarization division multiplexing (PDM) and CDM techniques, where n is the number of the code sequences. Each RRU has a code sequence (CS), which is orthogonal to other RRUs'. At the BBU, the downstream CDM signal and LO are transmitted over two SSMFs in parallel. The CDM signal is transmitted to every RRU by a 1:n optical splitter at the remote. By considering the power budget and fiber loss, 10 km SSMF and 1:8 optical splitter could be supported in the proposed system. Therefore, the system can support the transmission from BBU to at most 8 RRUs with a set of 8-bit CDM codes. At each RRU, the signal that belongs to itself is demultiplexed relying on the code sequence orthogonality. Finally, the demultiplexed signals of two polarizations are processed by the DSP module and then converted into the radio frequency (RF) signal transmitted by two antennas.

It is worth mentioning that the downstream fiber used to transmit the LO could also be used for the upstream transmission [26], [27]. As shown in Fig. 4, the first fiber (red) could support the downstream signal transmission while the second fiber (blue)

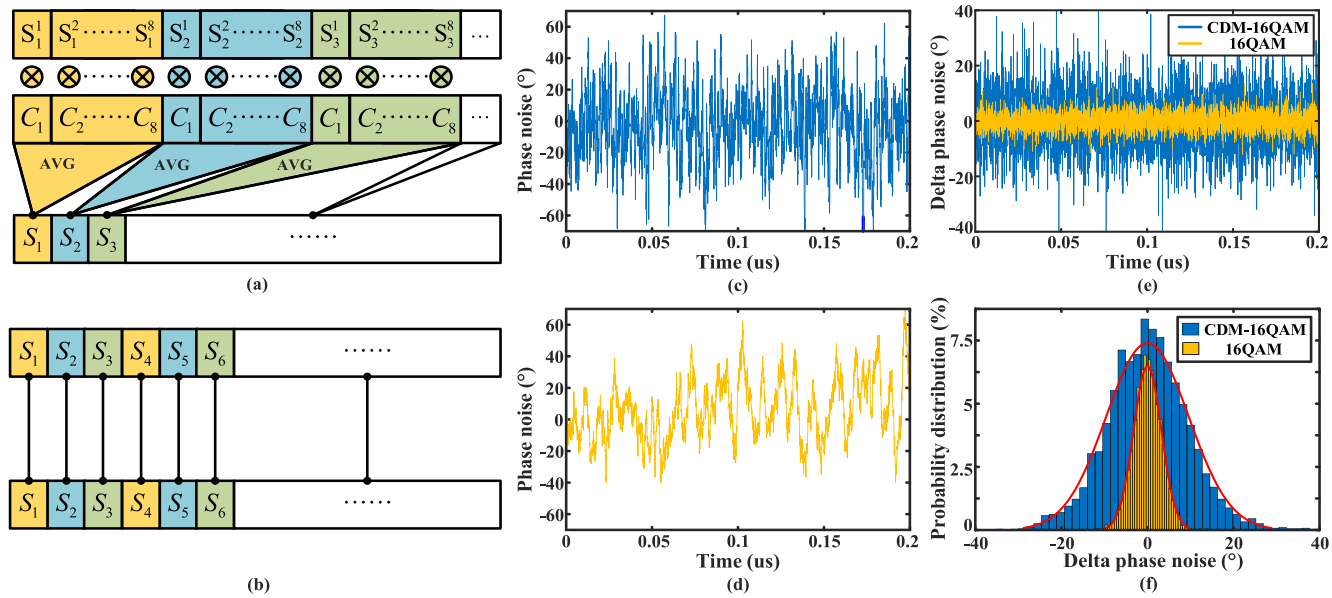

Fig. 5. The transmission process of CDM-16QAM signal (a) and 16QAM signal (b) in the SHC system. Phase noise of CDM-16QAM (c) and 16QAM (d) signal transmission. Delta phase noise between two symbols of CDM-16QAM and 16QAM (e) signal transmission. Delta phase noise distribution of CDM-16QAM and 16QAM (f) signal transmission.

could support both the downstream LO and the upstream signal. The same as the classical bidirectional transmission system, two fibers could support both the downstream and upstream transmission, which means the extra fiber used to transmit the LO in the proposed downstream system will not cause an extra cost to the whole MFH system, but we only discuss the downstream in this paper.

C. Pilot Sequence-Assisted CPR Algorithm

In the process of multiplexing in the CDM system, each channel's signal is spread firstly using its code sequence, which can be expressed as:

$$[s(1)s(2)\cdots s(7)s(8)] = S \cdot [C(1)C(2)\cdots C(7)C(8)] \quad (1)$$

where s represents an original signal symbol and $C(i)$ represents the i-th symbol of this channel's code sequence. Generally, $C(i)$ is 1 or -1. The left of (1) is defined as the spread signal sequence of S or a CDM chip. The spread signals of all the channels are added in the time domain and transmitted in parallel. The multiplexed signal will be affected by phase noise induced by laser linewidth and fiber length mismatch between the signal and LO paths in the SHC system, which can be described as:

$$CDM_{block} = \begin{pmatrix} s_1(1)e^{j\varphi_1} & s_1(2)e^{j\varphi_2} & \cdots & s_1(7)e^{j\varphi_7} & s_1(8)e^{j\varphi_8} \\ + & + & + & + & + \\ \vdots & \vdots & \vdots & \vdots & \vdots \\ + & + & + & + & + \\ s_8(1)e^{j\varphi_1} & s_8(2)e^{j\varphi_2} & \cdots & s_8(7)e^{j\varphi_7} & s_8(8)e^{j\varphi_8} \end{pmatrix} \quad (2)$$

where $S_m(n)$ represents the n-th symbol in the CDM chip of channel m and φ_n represents the phase noise of the n-th symbol. The multiplexed signal sequences of 8 CDM chips are defined as one CDM block. Noticed that each channel has 8 spread signal symbols in a CDM chip because an 8-bit CDM code is used in the proposed system. The process of demultiplexing is shown in Fig. 5(a). Based on the orthogonality of the CDM code, an RRU's signal can be demultiplexed from the CDM signal by the correlation operation between CDM blocks and its code sequence, which can be presented as:

$$S = \frac{1}{8} \cdot [C(1) \cdot CDM_{block}(1) + C(2) \cdot CDM_{block}(2) + \cdots\cdots + C(8) \cdot CDM_{block}(8)], \quad (3)$$

where $CDM_{block}(i)$ represents the i-th symbols in a CDM block. A demultiplexed signal symbol of channel m at the receiver can be expressed as:

$$S_r = S_m \cdot PN + \delta = S_m \left(\frac{1}{8} \sum_{n=1}^{8} e^{j\varphi_n} \right) + \delta, \quad (4)$$

where PN represents the phase noise and δ is the crosstalk noise. The process of demultiplexing relies on the orthogonality of code sequence. Each symbol transmitted in the channel is influenced by phase noise, and thus the complete orthogonality relation between different channels in a CDM block is broken, resulting in crosstalk noise δ. When the phase noise is small, the φ inside a CDM block can be regarded as a slowly varying value, so the damage to the code sequence orthogonality is negligible. If the phase noise is large, the φ inside a CDM block can no longer be regarded as a slowly varying value, and the crosstalk noise δ will be generated.

Compared with the traditional 16QAM signal transmission shown in Fig. 5(b), the change of phase noise between two demultiplexed symbols is much larger in the CDM-16QAM signal transmission, because it is the accumulation of delta phase

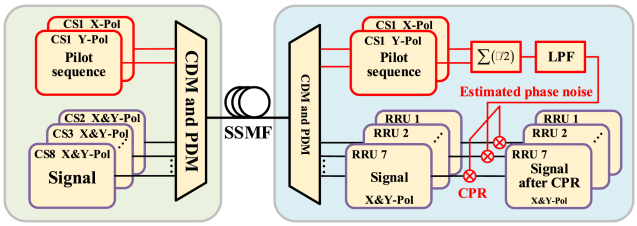

Fig. 6. Principle of the proposed pilot sequence-assisted CPR algorithm.

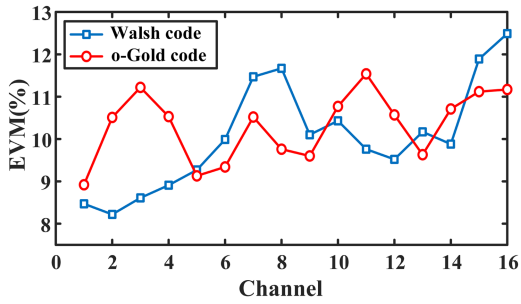

Fig. 7. The measured EVM performance of each channel using the Walsh code and orthogonal Gold code in simulation.

noise of n spread symbols. A 20 GBaud transmission simulation is carried out with CDM-16QAM signal and 16QAM signal, respectively. The laser linewidth is 4MHz and the mismatch length is 1m in this simulation. Fig. 5(c) and (d) show the phase noise of 4000 symbols in the CDM-16QAM and 16QAM signal transmission, respectively. The range of phase noise is nearly the same. But it is obvious that the delta phase noise of the demultiplexed CDM-16QAM signal is much larger than the 16QAM signal from Fig. 5(e) and (f). Therefore, it is difficult for the blind CPR algorithm to estimate the phase noise correctly because the blind CPR algorithm is mainly based on continuous slow change of phase noise.

To cope with this problem, a pilot sequence-assisted phase recovery algorithm is proposed as shown in Fig. 6, two of 16 channels (each polarization state has 8 channels) are used to transmit the pilot sequences and the rest 14 channels are used to transmit signals in this CDM-SHC system. The content of the pilot sequence does not need to be specially designed. In the CDM system, the signals of each channel are transmitted in parallel, so the phase noise of each channel's signal is nearly the same. Therefore, we chose two channels to transmit pilot sequences represented as $S_{\mathrm{T}}^{1}(n)$ and $S_{\mathrm{T}}^{2}(n)$. In the downstream, 16 channels are transmitted in parallel and finally transmitted to 7 RRUs through an optical splitter. The location of each RRU is different, therefore, after receiving the signal, each RRU needs to demultiplex its signal and two pilot sequences. The pilot sequences will carry phase noise information after the transmission, which can be described as:

$$\begin{aligned} S_{T\_rx}^{1}(n) &= S_{T}^{1}(n)\exp\left[j\varphi_1(n)\right], \\ S_{T\_rx}^{2}(n) &= S_{T}^{2}(n)\exp\left[j\varphi_2(n)\right]. \end{aligned} \tag{5}$$

Then we can estimate the phase noise of two pilot sequences by:

$$\varphi_i(n) = \arccos\left[\frac{S_T^i(n)\,S_{T,n}^i(n)^*}{|S_T^i(n)|\cdot|S_{T,n}^i(n)|}\right], (i=1,2). \tag{6}$$

The average of 2 phase noise curves is calculated to reduce the influence of the crosstalk noise δ.

$$\varphi(n) = \frac{\varphi_1(n)+\varphi_2(n)}{2}. \tag{7}$$

The phase noise curve is then smoothed by a low-pass filter (LPF). The LPF is a simple average filter and its number of taps is 3. The phase noise value of the CDM system is still continuously changing, although it changes faster than that of the 16-QAM system. By using this LPF, the estimation error of phase noise could be effectively removed, and the compensation performance can be increased. Finally, the carrier phase can be easily recovered by:

$$S_{rx\_CPR}^{1}(n) = S_{rx}^{1}(n)\exp\left[-j\varphi(n)\right]. \tag{8}$$

D. The Principle of Balancing the Transmission Performances Between Different RRUs

In the CDM system, RRUs are identified by orthogonal code sequences. The characteristic of each code sequence is different, and thus the transmission performance of each channel is not the same. To balance the signal quality between different RRUs, the CDM code needs to be optimized. Walsh code and orthogonal Gold code are widely used as CDM code [28]. The Walsh code is generated from Hadamard matrices. The Gold code is generated by shifting two m-sequences and adding them to module 2. The orthogonal Gold code can be generated by complementing 0 at the end of the generated Gold code [29].

The performance of the Walsh code and orthogonal Gold code is compared in a 20 GBaud simulation. In the simulation, a Chebyshev I-type filter at 20 GHz is used to emulate the 20 GHz bandwidth limitation. Fig. 7 shows the transmission performance of the CDM system using 8-bit CDM code. Channels 1 to 8 are X-polarization signals and Channels 9 to 16 are Y-polarization signals. The range of the measured EVM value using the Walsh code is larger than that using the orthogonal Gold code. For the Walsh code, Channel 16 has the worst EVM performance and Channel 2 has the best EVM performance, and the range of EVM values is around 4%. The EVM performances of the orthogonal Gold code are more balanced between channels. Channel 11 has the worst EVM performance, and Channel 1 has the best EVM performance. The range of EVM values is only 2.3%. The signal quality between different RRUs is more balanced when using the orthogonality Gold code. The reason could be explained by previous research that the orthogonal Gold code has high auto-correlation and lower cross-correlation compared with the Walsh code [30]. Therefore, we chose the orthogonality Gold code as the CDM code in the following simulation and experiment.

However, the transmission performances of 16 channels are still not balanced enough even using the orthogonal Gold code. The reason could be explained in the frequency domain as shown in Fig. 8, and each channel's spectrum of spread signals using

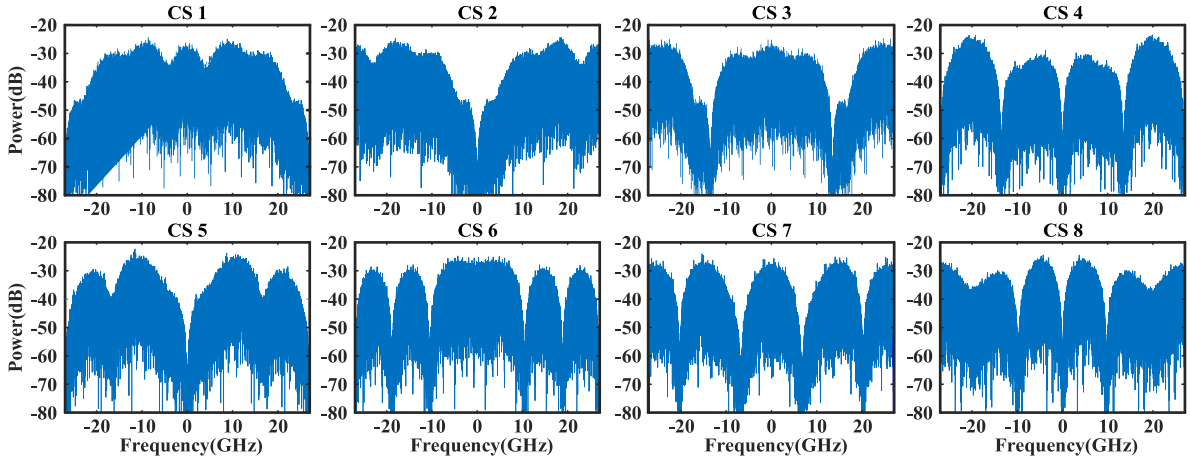

Fig. 8. The spectrum of spreading signals using different code sequences (CS) of orthogonal Gold code.

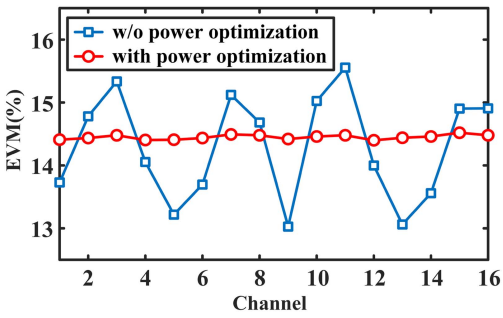

Fig. 9. The measured EVM performance of each channel with or without power optimization.

orthogonal Gold code is plotted. It's obvious that the spread signal's distribution in the frequency of each code sequence is different. Code sequences that contain fewer high-frequency components perform better, such as CS 1 and CS 5, which agrees with the simulation result shown in Fig. 7. Therefore, to ensure all the RRUs' transmission performances are balanced, it is necessary to optimize the system.

We propose a power optimization scheme to balance the performances of RRUs. The scheme is realized by multiplying each channel's signal by a normalized weight factor at the transmitter before the multiplexing operation. The normalized weight factor of each channel is optimized according to the actual experimental results. The normalized weight factor of the RRU with the worst performance is 1. As a result, the worst channel has a higher signal-to-noise ratio (SNR), contributing to improved transmission performance. Finally, the performances of all channels tend to be the same by optimizing the normalized weight factor of each channel. On this basis, a 35 GBaud signal transmission simulation using the orthogonal Gold code is carried out at the 20 GHz bandwidth limitation. Fig. 9 shows the measured EVM performance of each channel with or without power optimization in simulation. It can be observed that the range of EVM values is 2.5% without the power optimization scheme, and the best EVM performance is 13.0% while the worst EVM performance is 15.6%. With the help of power optimization, the EVM values of all the channels are all-around 14.5%.

III. Experimental Setup

The experimental setup of P2MP mobile Fronthaul downstream transmission using CDM and SCH technologies is shown in Fig. 10. At the transmitter, the data is generated offline using MATLAB. A pseudorandom bit sequence (PRBS) is produced and then mapped into 16QAM format. The 16QAM signal sequence is converted into 16 channels in parallel and processed by the proposed power optimization scheme. Subsequently, these 16 channels are divided into two groups, and each group has 8 channels. The generated 8-order orthogonal Gold code is assigned to these two groups. The two sets of channels are multiplexed by the PDM technology, so these two sets of channels can use the same set of CDM codes. Signals of 16 channels are spread with their code sequences, then the 8 spread signals of each group are added in the time domain to achieve digital code-division multiplexing. Subsequently, two CDM signals are generated, and each one is transmitted through a polarization state, containing signals of 8 channels. Two of the 16 channels are used to transmit the pilot sequence (one at the X polarization and the other one at the Y polarization). After being up-sampled by inserting zero between adjacent symbols, the CDM signals are pulse-shaped by a root-raised cosine filter with a oll-off of 0.1. The generated two CDM signals are loaded into a four-channel arbitrary waveform generator (AWG, Keysight M8195A) with a 3dB bandwidth of 20 GHz. The output peak-to-peak voltages of signals are set to 400mV, and the signals are amplified by a four-channel electrical amplifier (EA) with a gain of 24 dB. The amplified electrical signals are modulated on the optical carrier by a dual-polarization optical IQ modulator (DP IQM).

A DFB laser with a linewidth of 4 MHz and maximum output power of 14.5 dBm is used in this experiment. The output of this laser is divided into 2 parts through a 1:99 optical splitter. The 99% part is used as the signal optical carrier while the 1% part is used as the LO. The 16QAM signals of 16 channels are modulated on the optical carrier after multiplexing, then transmitted through 10 km SSMF. A variable optical attenuator (VOA) is placed after the 10 km SSMF to emulate the insert loss of an optical splitter. An integrated coherent receiver (ICR, FUJITSU-FIM24706/301) with the 3 dB bandwidth of 22 GHz

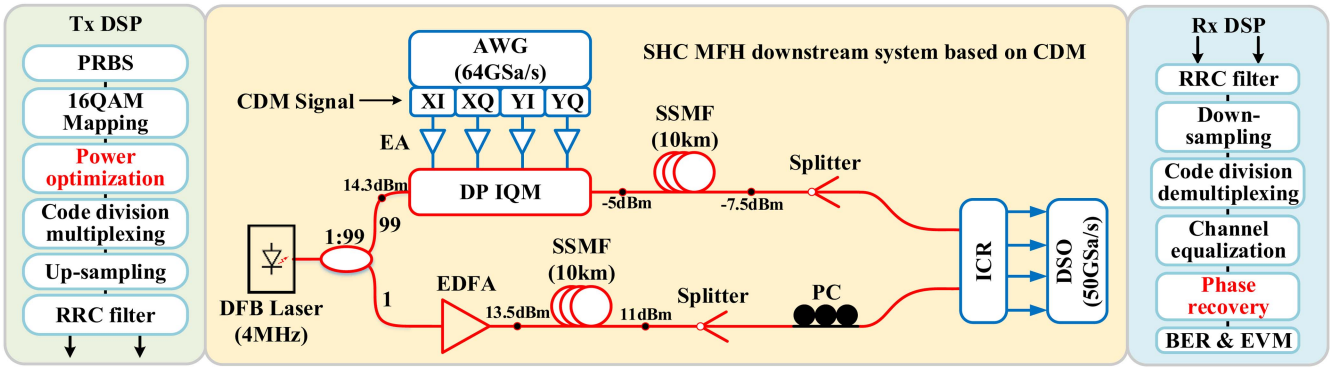

Fig. 10. The experimental setup of P2MP mobile Fronthaul downstream transmission using CDM and SCH technologies.

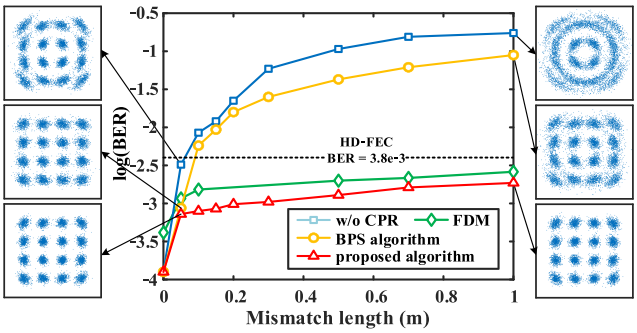

Fig. 11. The measured BER performance of the CDM (with the BPS algorithm, with the proposed CPR algorithm, and without any algorithms) and FDM in terms of different fiber mismatch lengths.

is used for coherent homodyne detection, and the output signal is captured by a digital sampling oscilloscope (DSO, Tektronix DPO-73304D) for the offline process. At the receiver, the signal is first passed through a root-raised cosine filter with a roll-off of 0.1, which is the same as the transmitter. After down-sampling, two CDM signals are obtained, corresponding to channels 1 to 8 and channels 9 to 16. Subsequently, these two CDM signals are demultiplexed. After channel equalization, the phase noise is estimated using the proposed algorithm. About 3.2×10^5 bits are used for EVM and BER counting.

IV. Results and Discussion

To verify the performance of the proposed CPR algorithm, a DFB laser with a linewidth of 4 MHz is used in our experiment, and the fiber mismatch length is emulated by changing the fiber length of the LO link. Since the emulated fiber mismatch lengths are all on the order of meter, the power loss caused by the change of fiber length can be ignored. The CDM code used in this experiment is orthogonal Gold code. Fig. 11 shows the measured BER performance of the 20 Gbaud CDM-16QAM signal in terms of different fiber mismatch lengths with the BPS algorithm, proposed CPR algorithm, and without any CPR algorithm. It can be observed that the measured BER cannot be below the HD-FEC threshold with the BPS algorithm when the fiber mismatch length is longer than 0.05 m, because of the large delta noise in the CDM-16QAM system. When the fiber mismatch length is 1m, the transmission performance has deteriorated greatly according to the constellation of the received signal as shown in the inset of Fig. 11. However, with the help of the proposed CPR algorithm, the BER performance is still below the HD-FEC threshold even when the fiber mismatch length is 1m. The tolerance of the product of laser linewidth and delay mismatch is improved from 0.2 MHz · m (0.05 m × 4 MHz) to 4 MHz · m (1 m × 4 MHz), which makes it possible to use low-cost DFB laser. Note that the constellation of the signal processed by the BPS algorithm is better than that without any CPR operation, but their BER values are similarly bad. The reason is that the large delta phase noise in the CDM system greatly affects the phase noise estimation process of the BPS algorithm, which causes the phase cycle-slip. That means the constellation points are corrected to the wrong position. Though these points are distributed around the ideal constellation point, the information they carried is totally wrong. Moreover, it can be observed that the BER performance still slightly deteriorates as the mismatch length increases even if the proposed CPR is used. The reason is that the orthogonality of the code sequence in a CDM block is broken more seriously when the induced phase noise becomes larger, leading to larger crosstalk noise δ. However, with the help of the proposed CRP algorithm, the fiber mismatch length tolerance can be improved from 0.05m to >1m at the HD-FEC threshold when a 4 MHz linewidth DFB laser is used. Also, for comparison, the BER performance of FDM under the phase noise is tested in the experiment. The OSNR and transmission bandwidth are the same as in the CDM experiment and the guard bandwidth of FDM is set to 0.5 GHz. The measured BER of the FDM is higher than that of the CDM even when the fiber mismatch length is the same. This is because the BER performance shown in Fig. 11 is the worst of all the channels, and the FDM has a higher channel performance difference due to the uneven amplitude-frequency response of the transmission system. But the BER penalty after carrier phase recovery is similar for CDM and FDM.

Fig. 12 shows the measured EVM performance of 35 Gbaud CDM-16QAM signal after 10 km SSMF transmission, and the Walsh code and orthogonal Gold code are both tested. In this experiment, the optical power of the LO and signal is 4 dBm and −20 dBm, respectively. The results are consistent with the simulation results in Fig. 7, and the EVM performance differences of

TABLE I
OPTIMAL NORMALIZATION WEIGHT FACTOR OF EACH CHANNEL

	Code 1	Code 2	Code 3	Code 4	Code 5	Code 6	Code 7	Code 8
X-Pol.	Channel 1	Channel 2	Channel 3	Channel 4	Channel 5	Channel 6	Channel 7	Channel 8
	0.82	0.91	0.90	0.88	0.82	0.83	0.91	0.87
Y-Pol.	Channel 9	Channel 10	Channel 11	Channel 12	Channel 13	Channel 14	Channel 15	Channel 16
	0.87	1.00	0.90	0.98	0.84	0.85	0.94	0.87

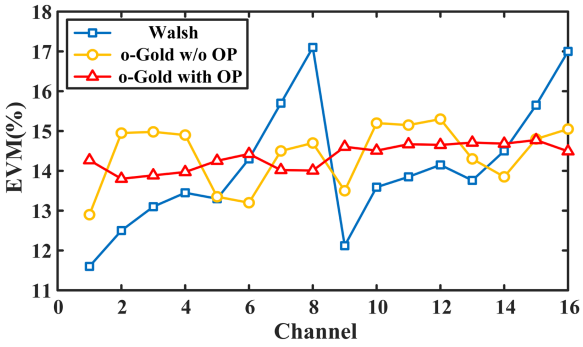

Fig. 12. The measured EVM performance of 35 Gbaud CDM-16QAM signal after 10 km SSMF transmission using the Walsh code and the orthogonal Gold code with or without power optimization.

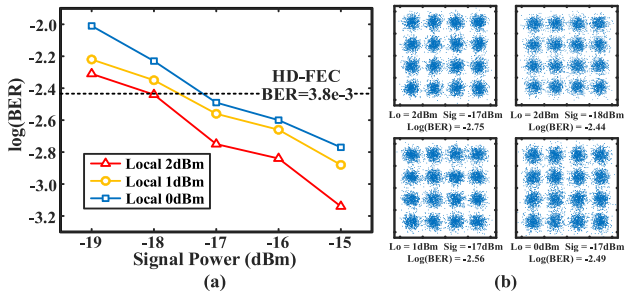

Fig. 13. The measured BER performance of 245 Gb/s CDM-16QAM signals in terms of the received signal optical power after 10 km SSMF transmission (a). The worst constellations of the received signals at different power setups (b).

all channels are relatively small when the orthogonal Gold code is used. The best EVM value is 12.9% and the worst EVM value is 15.4%. For the Walsh code, the EVM performance of different channels varies obviously, and the best EVM value is 11.5% and the worst EVM value is 17.2%. Therefore, the orthogonal Gold code has better transmission performance than the Walsh code in our experiment. Based on the above results, a power optimization algorithm is designed by multiplying each channel's signal by a normalized weight factor before the multiplexing at the transmitter. Note that the normalized weight factor of each channel only depends on the code sequence and the specific channel transmission environment. So, a set of normalized weight factors could work for quite a long time once it is determined through constant optimization. The optimal normalized weight factor of each channel obtained in our experiment is shown in Table I. Channel 1 to Channel 8 is transmitted at the X polarization, and Channel 9 to Channel 16 is transmitted at the Y polarization. It can be seen in Table I that the optimal normalized weight factors of the X channel and Y channel change similarly, and the reason is that they use the same code sequence. But the normalized weight factors of X polarization are smaller than Y polarization generally. This could be attributed to the different performances of optical and electrical components in these two branches. Fig. 12 also presents the measured EVM performance of 35 Gbaud CDM-16QAM signals with and without the power optimization. It could be observed that the range of the EVM values of different channels became smaller and the worst EVM value is reduced from 15.4% to 14.8% with the help of power optimization.

Finally, by using the proposed pilot sequence-assisted CPR algorithm and the power optimization scheme, a 245 Gb/s P2MP CDM-based MFH downstream transmission over 10 km SSMF is carried out. In this experiment, a DFB laser with a linewidth of 4 MHz is used, and the output power of this laser is 14.5 dBm. According to the measured optical power at different link points shown in Fig. 10, this system can support 7 RRUs (the insertion loss of the optical splitter is 9 dB). In the proposed MFH scenario, all the RRUs' BER performance should be below the FEC threshold. So, the performance of the worst channel needs to be focused on. Fig. 13(a) presents the measured worst BER performance of 245 Gb/s CDM-16QAM signals in terms of the received signal optical power after 10 km SSMF transmission. The receiver sensitivity at the HD-FEC limit (BER of 3.8×10^{-3}) is achieved at −17.2 dBm, −17.6 dBm, and −18.1 dBm for the LO optical power of 0 dBm, 1 dBm, and 2 dBm, respectively. The LO power of 2 dBm and signal power of −17 dBm could support the CDM-based downstream transmission with 7 RRUs. The constellations of the worst channel are shown in Fig. 13(b) at different power setups. Note that more RRUs could be supported if EDFA is used in the signal optical path.

V. CONCLUSION

In this paper, we have experimentally demonstrated a CDM and SHC-based P2MP mobile fronthaul downstream system from BBU to 7 RRUs. To reduce the cost and complexity of the system, a low-complexity phase noise estimation algorithm is proposed to increase the fiber length mismatch tolerance. To balance the signal quality between all the RRUs, the orthogonal Gold code is introduced, and a power optimization scheme is designed. Finally, a 245 Gb/s CDM-based MFH downstream transmission over 10 km SSMF is successfully achieved, and the linewidth of the used DFB laser is 4 MHz. The LO power of 2 dBm and signal power of −17 dBm could support the CDM-based downstream transmission with 7 RRUs. This research provides a potential solution for the high-speed mobile fronthaul in the future beyond 5G mobile communication system.

REFERENCES

[1] J. G. Andrews et al., "What will 5G be?," *IEEE J. Sel. Areas Commun.*, vol. 32, no. 6, pp. 1065–1082, Jun. 2014, doi: 10.1109/JSAC.2014.2328098.

[2] T. Pfeiffer, "Next generation mobile fronthaul and midhaul architectures [Invited]," *J. Opt. Commun. Netw.*, vol. 7, no. 11, pp. B38–B45, Nov. 2015, doi: 10.1364/JOCN.7.000B38.

[3] A. Pizzinat, P. Chanclou, F. Saliou, and T. Diallo, "Things you should know about fronthaul," *J. Lightw. Technol.*, vol. 33, no. 5, pp. 1077–1083, Mar. 2015, doi: 10.1109/JLT.2014.2382872.

[4] H. Ji, C. Sun, and W. Shieh, "Spectral efficiency comparison between analog and digital RoF for mobile fronthaul transmission link," *J. Lightw. Technol.*, vol. 38, no. 20, pp. 5617–5623, Oct. 2020, doi: 10.1109/JLT.2020.3003123.

[5] J. Kani, J. Terada, K.-I. Suzuki, and A. Otaka, "Solutions for future mobile fronthaul and access-network convergence," *J. Lightw. Technol.*, vol. 35, no. 3, pp. 527–534, Feb. 2017, doi: 10.1109/JLT.2016.2608389.

[6] A. Banerjee et al., "Wavelength-division-multiplexed passive optical network (WDM-PON) technologies for broadband access: A review [Invited]," *J. Opt. Netw.*, vol. 4, no. 11, pp. 737–758, Nov. 2005, doi: 10.1364/JON.4.000737.

[7] K. Honda et al., "Wavelength control method of upstream signals using AMCC in WDM-PON for 5G mobile fronthaul," *Opt. Exp.*, vol. 27, no. 19, pp. 26749–26756, Sep. 2019, doi: 10.1364/OE.27.026749.

[8] J. Zou, C. Wagner, and M. Eiselt, "Optical fronthauling for 5G mobile: A perspective of passive metro WDM technology," in *Proc. Opt. Fiber Commun. Conf.*, Los Angeles, CA, USA, 2017, pp. 1–3.

[9] D. J. Richardson, J. M. Fini, and L. E. Nelson, "Space-division multiplexing in optical fibres," *Nature Photon.*, vol. 7, no. 5, pp. 354–362, May 2013, doi: 10.1038/nphoton.2013.94.

[10] B. J. Puttnam, G. Rademacher, and R. S. Luís, "Space-division multiplexing for optical fiber communications," *Optica*, vol. 8, no. 9, pp. 1186–1203, Sep. 2021, doi: 10.1364/OPTICA.427631.

[11] S. Bidkar, J. Galaro, and T. Pfeiffer, "First demonstration of an ultra-low-latency fronthaul transport over a commercial TDM-PON platform," in *Proc. Opt. Fiber Commun. Conf.*, San Diego, CA, USA, 2018, pp. 1–3.

[12] S. Zhou, X. Liu, F. Effenberger, and J. Chao, "Low-latency high-efficiency mobile fronthaul with TDM-PON (Mobile-PON)," *J. Opt. Commun. Netw.*, vol. 10, no. 1, pp. A20–A26, Jan. 2018, doi: 10.1364/JOCN.10.000A20.

[13] A. Gatto, P. Parolari, and P. Boffi, "Frequency division multiplexing for very high capacity transmission in bandwidth-limited systems," in *Proc. Opt. Fiber Commun. Conf.*, Los Angeles, CA, USA, 2017, pp. 1–3.

[14] B. Baeuerle, A. Josten, M. Eppenberger, D. Hillerkuss, and J. Leuthold, "Low-complexity real-time receiver for coherent Nyquist-FDM signals," *J. Lightw. Technol.*, vol. 36, no. 24, pp. 5728–5737, Dec. 2018, doi: 10.1109/JLT.2018.2877479.

[15] L. Dou et al., "420Gbit/s DP-64QAM Nyquist-FDM single-carrier system," in *Proc. Opt. Fiber Commun. Conf.*, Anaheim, CA, USA, 2016, pp. 1–3.

[16] A. Gatto, P. Parolari, and P. Boffi, "FDM exploitation for next access and data networks," in *Proc. 19th Int. Conf. Transp. Opt. Netw. (ICTON)*, Girona, Spain, 2017, pp. 1–4. doi: 10.1109/ICTON.2017.8024854.

[17] H. Li et al., "Digital code-division multiplexing channel aggregation for mobile fronthaul architecture with low complexity," *IEEE Photon. J.*, vol. 10, no. 2, pp. 1–10, Apr. 2018, doi: 10.1109/JPHOT.2017.2751538.

[18] Y. Tu, Z. Yang, S. Fu, and Y. Qin, "Latency-efficient code-division multiplexing (CDM) based carrier aggregation for 5G NR mobile fronthaul," *Opt. Commun.*, vol. 472, Oct. 2020, Art. no. 126051, doi: 10.1016/j.optcom.2020.126051.

[19] D. Che, "Analog vs digital radio-over-fiber: A spectral efficiency debate from the SNR perspective," *J. Lightw. Technol.*, vol. 39, no. 16, pp. 5325–5335, Aug. 2021, doi: 10.1109/JLT.2021.3102220.

[20] B. Puttnam et al., "Self-homodyne detection in optical communication systems," *Photonics*, vol. 1, no. 2, pp. 110–130, May 2014, doi: 10.3390/photonics1020110.

[21] X. Chen, S. Chandrasekhar, and P. Winzer, "Self-coherent systems for short reach transmission," in *Proc. Eur. Conf. Opt. Commun. (ECOC)*, Rome, Italy, 2018, pp. 1–3, doi: 10.1109/ECOC.2018.8535234.

[22] I. Alimi et al., "A review of self-coherent optical transceivers: Fundamental issues, recent advances, and research directions," *Appl. Sci.*, vol. 11, no. 16, Aug. 2021, Art. no. 7554, doi: 10.3390/app11167554.

[23] X. Zhou, Y. Gao, J. Huo, and W. Shieh, "Theoretical analysis of phase noise induced by laser linewidth and mismatch length in self-homodyne coherent systems," *J. Lightw. Technol.*, vol. 39, no. 5, pp. 1312–1321, Mar. 2021, doi: 10.1109/JLT.2020.3038213.

[24] S. Ishimura, Y. Nakano, and T. Tanemura, "Impact of laser phase noise on self-coherent transceivers employing high-order QAM formats," *J. Lightw. Technol.*, vol. 39, no. 19, pp. 6150–6158, Oct. 2021, doi: 10.1109/JLT.2021.3097092.

[25] J. Lu, S. Fu, M. Tang, M. Xiang, P. Shum, and D. Liu, "Low-complexity carrier phase estimation for M-ary QAM based on blind phase search using simplified measurement," in *Proc. 15th Int. Conf. Opt. Commun. Netw. (ICOCN)*, Hangzhou, China, 2016, pp. 1–3. doi: 10.1109/ICOCN.2016.7875658.

[26] L. Wang et al., "First real-time MIMO-free 800Gb/s DP-64QAM demonstration using bi-directional self-homodyne coherent transceivers," in *Proc. Eur. Conf. Opt. Commun.*, WA, DC, USA, 2021, Paper PD1.5.

[27] T. Gui, X. Wang, M. Tang, Y. Yu, Y. Lu, and L. Li, "Real-time demonstration of homodyne coherent bidirectional transmission for next-generation data center interconnects," *J. Lightw. Technol.*, vol. 39, no. 4, pp. 1231–1238, Feb. 2021, doi: 10.1109/JLT.2021.3052826.

[28] E. H. Dinan and B. Jabbari, "Spreading codes for direct sequence CDMA and wideband CDMA cellular networks," *IEEE Commun. Mag.*, vol. 36, no. 9, pp. 48–54, Sep. 1998, doi: 10.1109/35.714616.

[29] L. Shufeng, H. Shiyao, and W. Hongda, "Analysis of DS-CMDA system using orthogonal gold sequence," in *Proc. IEEE 7th Int. Conf. Electron. Inf. Emerg. Commun. (ICEIEC)*, Macau, China, 2017, pp. 520–523. doi: 10.1109/ICEIEC.2017.8076619.

[30] G. V. S. Raju and J. Charoensakwiroj, "Orthogonal codes performance in multi-code CDMA," in *Proc. IEEE SMC'03 Conf. Int. Conf. Syst., Man Cybern.. Conf. Theme - System Secur. Assurance (Cat. No.03CH37483)*, Oct. 2003, vol. 2, pp. 1928–1931. doi: 10.1109/ICSMC.2003.1244693.